

2-DOF Contactless Distributed Manipulation Using Superposition of Induced Air Flows

Anne Delettre, Guillaume J. Laurent and Nadine Le Fort-Piat

Abstract—Many industries require contactless transport and positioning of delicate or clean objects such as silicon wafers, glass sheets, solar cell or flat foodstuffs. The authors have presented a new form of contactless distributed manipulation using induced air flow. Previous works concerned the evaluation of the maximal velocity of transported objects and one degree-of-freedom position control of objects. This paper introduces an analytic model of the velocity field of the induced air flow according to the spatial configuration of vertical air jets. Then two degrees-of-freedom position control is investigated by exploiting the linearity property of the model. Finally the model is validated under closed-loop control and the performances of the position control are evaluated.

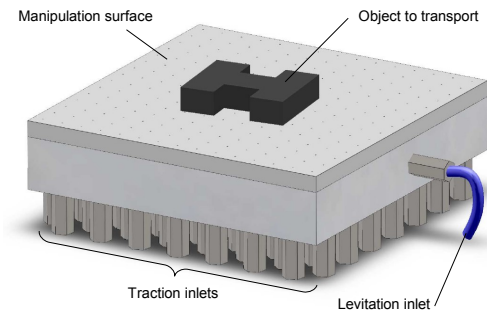
I. INTRODUCTION

Many industries require contactless transport and positioning of delicate or clean objects such as silicon wafers, glass sheets, solar cell or flat foodstuffs. The handling of delicate, freshly painted, hot, sensitive or micron-sized structured components is feasible because mechanical contact is avoided. Furthermore, dry friction forces are cancelled, which enables high velocity motions.

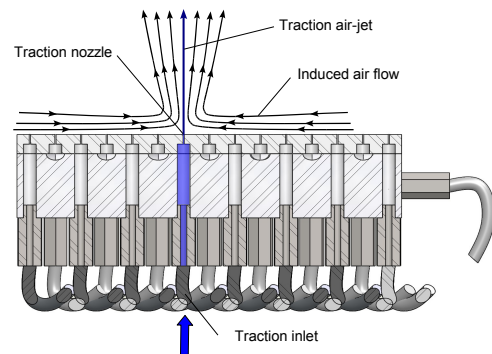
Researchers have experimented a variety of air-jet techniques to design contactless manipulators as air cushion or Bernoulli levitation. Because air flow is magnetic free and generates little heat, pneumatic approaches can be applied to any material: insulator or conductor, magnetic or non-magnetic, rigid or non-rigid. In air cushion levitation, the sample is held on a plate which is drilled by many small holes. Pressurized air flows upward through these holes and create an air cushion that counterbalances the weight of the component. This is the principle of popular air-hockey tables. Three approaches have been proposed to move the object: suction, tilted air jets and induced air flow.

Luntz and Moon [1], [2], [3], [4] use an air-hockey table in addition to a few flow sinks (suction points) above the table. The sinks create a stable flow pattern towards them. This device is a sensorless positioning surface able to move any rectangular object to a predictable orientation and position. Ku *et al.* [5] developed the same idea but they used closed-loop control to move the object from one sink to another.

Many devices use arrays of tilted air jets to produce a traction force in addition to the air cushion. The geometry of the device is designed to get stable transport system without closed-loop control, for example we can mention wafer and glass transportation systems [6], [7], [8]. In



(a) Global view



(b) Cross view showing the generation of the induced air flow (the path of the air flow is darkened).

Fig. 1. The induced air flow surface.

contrast, the Xerox PARK paper handling system [9], [10] uses 1,152 directed air jets in a 12 in. \times 12 in. array to levitate paper sheets. Each jet is separately controlled by an independent MEMS-like valve. The system has demonstrated closed-loop positioning accuracies in the order of 0.05 mm and trajectory tracking with typical velocity about $30 \text{ mm}\cdot\text{s}^{-1}$. Rij *et al.* [11] proposed a similar wafer transport system based on viscous traction principle. On a near microscopic scale, some active surfaces have been developed using MEMS actuator arrays. The surface of Fukuta *et al.* [12] is able to produce tilted air jets thanks to integrated electrostatic valves. Recently, Zeggari *et al.* [13] presented a passive pneumatic micro-conveyor that generates arrays of titled air jets for fast transport.

The authors have presented a new principle of aerodynamic traction using induced air flow [14], [15]. The induced air flow surface is a 120 mm \times 120 mm square surface drilled by two kinds of holes (cf. Fig. 1a). The object is maintained

A. Delettre, G. J. Laurent, and N. Le Fort-Piat are with the Automatic Control and Micro-Mechatronic Systems Department, FEMTO-ST Institute, UFC-ENSMM-UTBM-CNRS, Université de Franche-Comté, Besançon, France, {Firstname.Lastname}@ens2m.fr

in constant levitation thanks to the air cushion created by the airflow that comes through a common air inlet. The novelty is that the object can be moved on the table by generating strong *vertical* air jets through specific holes of the surface. These vertical air jets create an induced air flow in the surrounding fluid that pulls the object towards the nozzle (cf. Fig. 1b). Each nozzle is driven by an independent solenoid valve. Thus an object can be transported by opening successively the appropriate valves. Contrary to the device of Luntz and Moon, the induced air flow principle does not create stable equilibrium positions and then can not operate without active control. But our device is only composed of one table whereas the one of Luntz and Moon needs an air manipulator palm above the air table. Moreover our device is more precise and manipulation can be achieved faster.

Previous works have concerned the evaluation of the maximal velocity of transported objects [15] and one degree-of-freedom (DOF) position control of objects [14]. This paper introduces in section II an analytic model of the velocity field of the induced air flow according to the spatial configuration of vertical air jets. Then, in section III, two degree-of-freedom position control is investigated by exploiting the linearity property of the model. Model parameters are identified in section IV. And finally the model is validated under closed-loop control and the performances of the position control are evaluated in section V.

II. INDUCED AIR FLOW MODELING

To appreciate the potential of air-jet arrays for handling, it is first necessary to understand the basic characteristics of a single air-jet. The fundamental characteristics of turbulent liquid or gas jets have been described by Abramovich [16]. This jet structure has been extensively confirmed by experiments [17], [18].

A. Air-jet fundamentals

In the simplest case of a jet discharging fluid with a uniform initial velocity field U_e into a motionless medium, the boundary layer thickness in the initial section of the jet is zero, see Fig. 2. The boundary layer thickens away from the discharge point as particles of the surrounding medium become entrained and are carried along with corresponding particles of the jet which are slowed down. Whilst this leads to an increase in cross-section of the jet it also gradually “consumes” the non-viscous core. This short region of the jet in which the center line velocity remains constant is called the zone of flow establishment.

In this area, the axial velocity is given by:

$$U(z, r) = \begin{cases} U_e & \text{for } r \leq R(z) \\ U_e \exp \left[-\frac{(r-R(z))^2}{b^2(z)} \right] & \text{for } r \geq R(z) \end{cases} \quad (1)$$

where (z, r) are the axial and radial co-ordinates, U_e is the exit velocity, $b(z) = \beta z$ is the radius of the jet which spreads linearly, β is an experimental constant ($\beta = 0.114$), $R(z) = \frac{D}{2} - \frac{\beta}{\sqrt{2}}z$ is the radius of the core and D the diameter of the circular orifice.

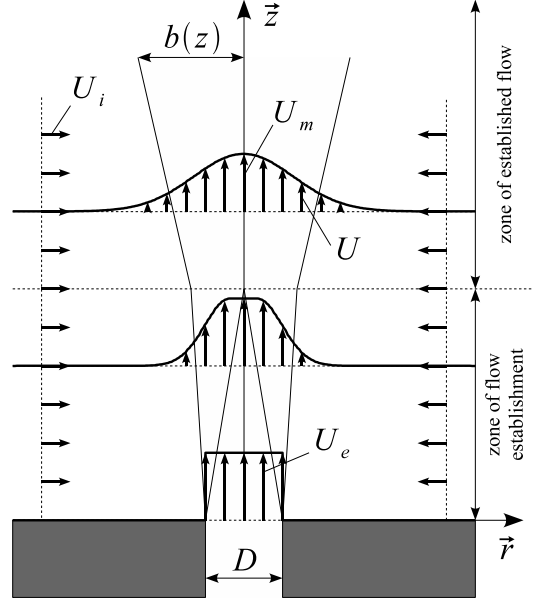


Fig. 2. Velocity profiles in a jet.

The plane representing the limit of constant axial velocity is called the transitional cross-section ($z = \frac{D}{\beta\sqrt{2}}$). Beyond this point in the zone of established flow, the center line velocity of the jet U_m gradually reduces as the diameter of the jet continues to expand.

$$U_m = U_e \frac{D}{\sqrt{2}b(z)} \quad (2)$$

In this area, the axial velocity profile is then:

$$U(z, r) = U_m \exp \left[-\frac{r^2}{b^2(z)} \right] \quad (3)$$

In the zone of established flow, the volume flux along the axis of the jet at z and r is:

$$Q(z, r) = \int_0^r 2\pi y U(z, y) dy \quad (4)$$

$$= \frac{\pi U_e D}{\sqrt{2}} \left(1 - \exp \left[-\frac{r^2}{b^2(z)} \right] \right) b(z) \quad (5)$$

The inflowing entrainment flow at r (induced surface flow) is then:

$$\Lambda(r) = \frac{d}{dz} Q(z, r) \quad (6)$$

For $r > b(z)$, Λ is nearly constant:

$$\Lambda_{r>b} \approx \frac{\pi\beta U_e D}{\sqrt{2}} \quad (7)$$

The entrainment velocity for $r > b(z)$ is then:

$$U_i(r) = -\frac{\Lambda}{2\pi r} \approx -\frac{\beta U_e D}{2\sqrt{2}r} \quad (8)$$

The conclusion is that a vertical air jet can be assimilated to a sink (suction point) when $r > b(z)$.

B. Potential flow fields

The induced-air-flow surface enables to control individually the generation of vertical air jets. Assuming that the fluid is inviscid (that can be considered as true a few millimeters away from the orifice) and incompressible, the potential flow theory [19] predicts flow patterns depending on the position of the suction points (here the air jets).

Indeed, the velocity vector field \vec{U}_i is equal to the negative gradient of the two dimensional scalar potential function Φ :

$$\vec{U}_i = -\vec{\nabla}\Phi \quad (9)$$

According to Eq. 8, the potential function Φ is given by:

$$\Phi = \sum_{i=1}^k \frac{\Lambda_i}{2\pi} \ln(r_i) \quad (10)$$

where Λ_i is the strength of the i^{th} sink given by Eq. 7 and r_i is the distance from the i^{th} sink. The velocity vector flow fields can then be re-written as a sum:

$$\vec{U}_i = \sum_{i=1}^k \frac{\Lambda_i}{2\pi r_i} \vec{e}_i \quad (11)$$

where \vec{e}_i is the unit vector which gives the direction to the i^{th} sink.

If only one air jet is active, the corresponding velocity vector flow field can be represented as in Fig. 3a. We can note that the fluid flows directly toward the sink with the velocity increasing close to the sink following Eq. 11.

C. Flow shaping

Let's now see what happens with a combination of air jets. When several air jets are active, the resulting potential function is simply the sum of the individual sink potential functions. Our idea is to form the desired flow to move an object by choosing the appropriate combination of jets.

Fig. 3 gives several examples of velocity fields produced by different jets configurations. For instance, a y-directed line of jets produces a x-directed flow (Fig. 3c). The velocity of the x-directed flow can be increased by using more y-directed lines (Fig. 3d).

As the velocity field is the sum of simpler fields, the combination of a x-directed line and a y-directed line produces a 45°-oriented flow (Fig. 3e). Other orientations can be achieved by using other lines combinations (in Fig. 3f the flow is oriented of 28° from x-direction).

More flow strength and orientations could be achieved by using other combinations of lines. In this paper, we propose to focus on these configurations (x-oriented and y-oriented lines) to validate the modeling and to perform 2-DOF control. The exhaustive flow shaping and 3-DOF control is left for future work.

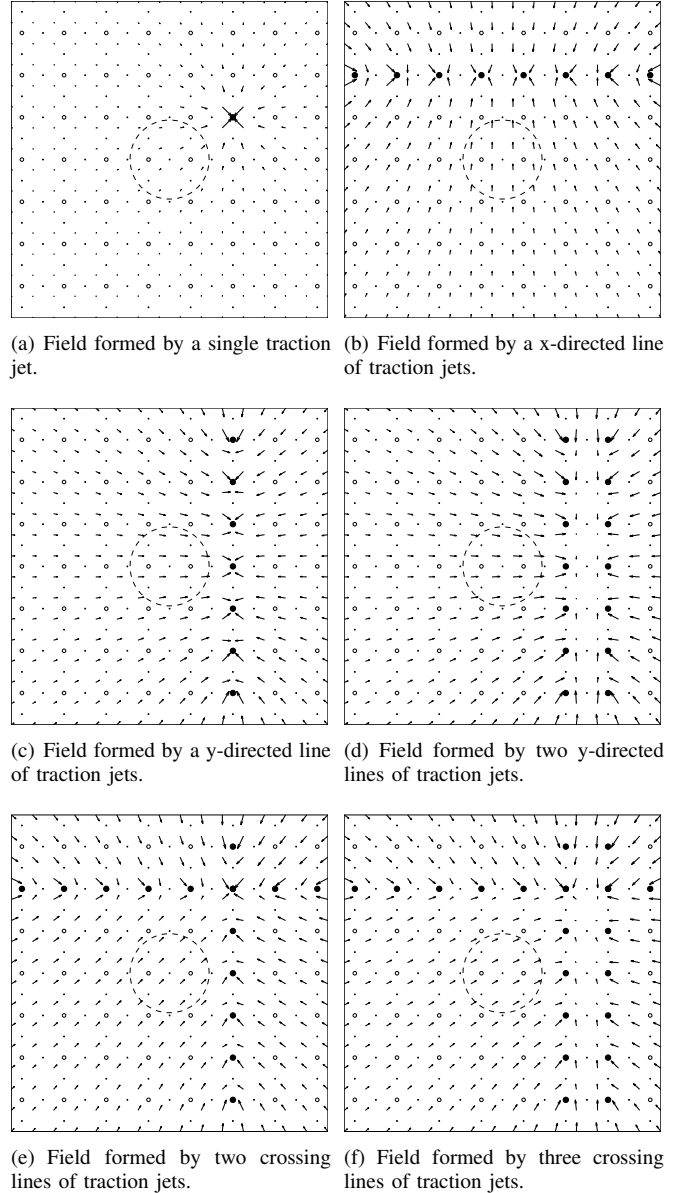


Fig. 3. Top-view of the induced air flow surface for different jets configurations (small black dots represent levitation nozzles, white circles represent closed traction nozzles, black circles represent opened traction nozzles, dashed line represents the shadow of the manipulated object and arrows represent the velocity of the air flow).

III. 2-DOF POSITION CONTROL

A. 1-DOF position control

In previous works [14], 1-DOF position control has been experimented on the same device using a PID controller. We chose to control y-directed lines of jets in order to control the x-position of objects. The control signal u_x represented the number of column(s) of air jets to enable (given by its rounded absolute value), and their x-position relative to the object's one (given by its sign). For example, the control signal corresponding to the pattern of Fig. 3c is $u_x = +1$ since the object is on the west of the jets and there is one line of jets. In Fig. 3d, the control signal is $u_x = +2$.

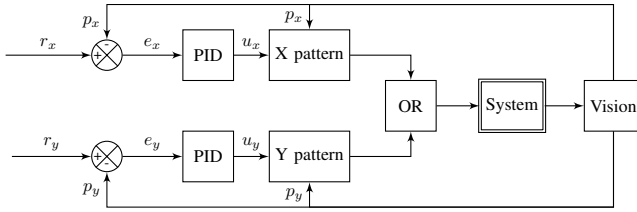


Fig. 4. Control architecture.

Furthermore, the minimal distance between the object and the closest jet was experimentally fixed to 8 mm. This distance is sufficient to prevent from complex turbulent flows that can occur when the object is very closed to an air jet.

B. 2-DOF position control

We now extend the control to 2 degrees of freedom using the same principle and the same controllers. Indeed, the potential function Φ is a linear function of the number of sinks (see Eq. 10). Thus the two dimension controls can be treated separately as the potential function resulting from the combination of several lines of jets is the sum of the individual potential functions. In other words, as represented in Fig. 4, one PID controls the x-position p_x of the object and one PID controls its y-position p_y . The controllers give respectively the number of y-directed and x-directed lines of air jets to enable and their position(s) relative to the object. For example, the control signals in the patterns of Fig. 3b, 3e and 3f are respectively $(u_x = 0; u_y = +1)$, $(u_x = +1; u_y = +1)$ and $(u_x = +2; u_y = +1)$.

The PID controllers are tuned with the same coefficients, as the distance between two nozzles along the two directions is the same (16 mm). The “X pattern” and “Y pattern” blocks calculate the distribution map of the 56 traction nozzles on the surface. They give the position of the nozzles to open depending on the number of y-oriented lines and x-oriented lines to enable and the position of the object. The OR block combines the two patterns using the logical or operator in order to send a unique pattern to the system corresponding to the air jets to enable.

We can note from Fig. 3 that if the reference position of the object during the control is near the middle of the active surface, the two dimension controls are not coupled.

IV. MODEL IDENTIFICATION

A. Induced surface flow identification

In order to apply Eqs. 7 and 11 and to derive equations that can predict air-jet forces we need to know the exit jet velocity U_e that can be expected from a given supply pressure. The answer is not straightforward first because even at relatively low differential pressures the compressibility of air results in a supersonic flow and secondly because small pipes and small solenoid valves cause pressure drop along the air travel.

The straightforward application of the theory of compressible flow [19] does not give satisfactory results. The resulting values are overestimated because it does not take into account pressure drops in pipes and valves. We choose an alternative

way to identify the exit velocity based on the measurement of the mass flow.

For non-critical flows, U_e can be calculated from the mass flow conservation:

$$U_e = \frac{4\dot{m}_e}{\rho\pi D^2} \quad (12)$$

where \dot{m}_e is the mass flow, ρ is the density of the fluid (here the air) and $D = 0.4$ mm the orifice diameter.

For critical flows, the initial velocity U_e is limited to the speed of sound in air noted a and calculated at atmospheric pressure and density. However, while U_e cannot exceed ambient sonic velocity due to the formation of a shock wave, the mass flow rate of the jet continues to increase in proportion to the pressure. Continuity dictates that the effective area of the jet must abruptly increase in the plane of the shock. For critical flows the equivalent effective jet diameter D_c can be calculated from:

$$D_c = \sqrt{\frac{4\dot{m}_e}{\rho\pi a}} \quad (13)$$

Table I gives the identified values of equivalent diameter, velocity and surface flow for both the traction pressure and the levitation pressure. The values for the traction inlet are mean values. Indeed, in order to take into account fabrication variations of nozzles and valves, the mass flow has been measured for each traction nozzle and the corresponding surface flows have been calculated.

B. Dynamic of the object

As the object is levitating on an air cushion induced by the levitation air jets, no dry friction is applied on it. Moreover we focus in this paper on thick cylindrical objects. The main force experienced by the object moving through a fluid is then the drag force, given by:

$$\vec{F} = -\frac{1}{2}\rho AC_D \|\vec{V}_{rel}\| \vec{V}_{rel} \quad (14)$$

where A is the frontal area of the object, C_D is the drag coefficient and \vec{V}_{rel} is the velocity of the object relative to the fluid. The drag coefficient C_D depends on the geometry of the object and on the velocity of the fluid. Then from the value of the drag force applied on the object, we can deduce the acceleration of the object following the law of motion.

Note that nor the dynamic of the establishment of the air flow nor the dynamic of solenoid valves have been included in the model since they are very faster in comparison with the dynamic of the object.

C. Drag coefficient identification

As mentioned in previous section, the drag coefficient depends on both the geometry of the object and the velocity of the air. We have identified it experimentally for a cylindrical aluminum object and for different values of the air velocity. These values are given in Fig. 5 and have been interpolated in order to give the drag coefficient for any air velocity.

TABLE I
SURFACE FLOW FOR EACH AIR INLET PRESSURE (TRACTION AND LEVITATION)

Air inlet	Inlet pressure (Pa)	Mass flow (kg/s)	Exit velocity (m/s)	Equivalent diameter (m)	Surface flow (m ² /s)
Traction	5e5	1.35e-4	343	6.44e-4	5.592e-2
Levitation	1.5e4	5.82e-6	38.5	4.00e-4	3.895e-3

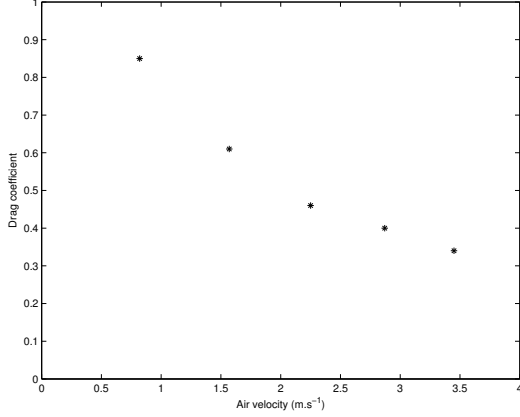


Fig. 5. Experimental drag coefficient depending on the air velocity.

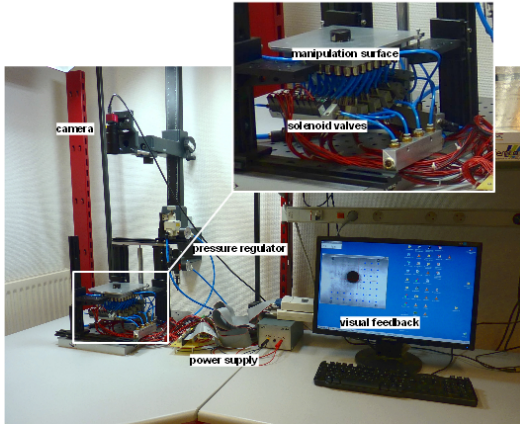


Fig. 6. Overview of the experimental setup.

V. EXPERIMENTAL RESULTS

A. Experimental setup

The experimental setup for the induced air flow surface is composed of pressurized air supply, two pressure regulators, the set of 56 solenoid valves and its control system, and a computer for vision processing. Fig. 6 describes the complete hardware configuration. The position of the holes is given in Fig. 3.

The induced air flow surface is put on a mechanical platform to adjust its equilibrium position. Default settings for operating pressures are 15 kPa for levitation and 500 kPa for traction. The valves are independently actuated through a multi-channel digital output board (NI USB-6509) and a 5V/24V amplifier circuit. A camera is used to grab video frames of the surface of the manipulator. The image processing is done by a computer at the rate of 60 frames per second (the software is cvLink).

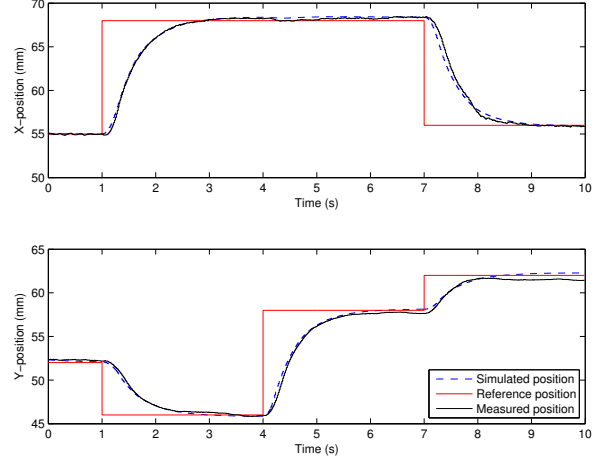


Fig. 7. Validation of the model: comparison between the measured position of the object and the simulated one under closed loop control thanks to PID controllers.

B. Validation of the model

The two dimensional model of the active surface has been validated experimentally (with the object mentioned before) in closed loop since the system is not stable. We used a cylindrical object so that its orientation does not influence the effect of the air on its displacement.

The input of our model is the position of the active air jets and the output is the position of the object on the active surface. Fig. 7 shows the comparison between the measured position of the object and the simulated one. Both plots are very closed: the system is pretty well modeled. Note that the system is perturbed by the ambient air flows, what can justify the variation between the model and the system responses. Furthermore, we can note a small static error in the y-direction because the valves linked to a same x-directed line of sinks are supplied by the same air inlet what might cause pressure drop.

C. 2-DOF position control

The control detailed in section III has been simulated and tested experimentally (Fig. 7). The proportional, integral and derivative coefficients of both PID controllers are respectively: $K_P = 2$, $K_I = 0.15$ and $K_D = 1$. They have been tuned by trial-and-error in previous work [14]. Results are shown in Fig. 7: the measured position of the object is compared to the simulated one. They can be further appreciated in the video clip accompanying this paper¹.

The experimental settling time is about 1.5 s. Small overshoot (less than 5%) appears sometimes because of the

¹Also available at <http://www.femto-st.fr/~guillaume.laurent/>

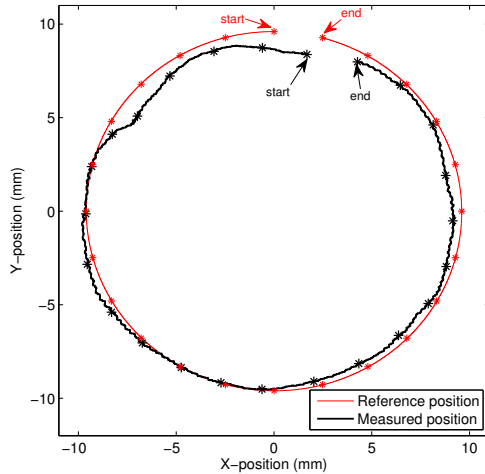


Fig. 8. Tracking results: the reference signal is a circle in the plan of the surface (crosses represent half-seconds).

discretization of the control signal and the minimal distance of 8 mm between the edge of the object and the nearest sink. The final position of the object varies in a maximal range of 100 μm .

We can note from these results that the two dimensions are nearly uncoupled. For example, after one second of running, the x-reference signal changes whereas the y-reference one does not. The object moves to the x-reference and its y-position is not too perturbed.

We have also experienced tracking: results are shown in Fig. 8. The performances are quite good, but we can note a tracking error of less than 2 mm for a speed motion value of 5.03 mm/s. Performances in tracking could be improved adapting the controller to this aim.

The PID controllers robustness has been evaluated using other objects: the system is stable and gives good performances for different objects (see the video clip mentioned before).

VI. CONCLUSIONS AND FUTURE WORKS

In this paper, we have modeled a contactless distributed manipulator using potential flow fields theory and validated this model experimentally. The model is able to predict the position of the object according to the position and the strength of the air jets. We have implemented two PID controllers to control two degrees of freedom of objects levitating on the active surface, using the fact that the two dimensions are not coupled. The position control has been experimented on the device and gives good performances: overshoot less than 5% and settling time around 1.5 s, although the system is heavy perturbed. The control of the rotation in the plan will be treated in future works, modeling the moment generated by the superposition of air jets.

We also prospect to miniaturize the device in order to adapt the manipulation principle to millimeter-sized objects (useful in pharmaceutical or watchmaker industries).

VII. ACKNOWLEDGMENT

This work was partially supported by the Smart Blocks NRA (French National Research Agency) project. The authors gratefully acknowledge Joël Agnus, David Guibert and Michaël Monasse from the FEMTO-ST Institute for their technical assistance.

REFERENCES

- [1] J. Luntz and H. Moon, "Distributed manipulation with passive air flow," in *Proc. of the IEEE Int. Conf. on Intelligent Robots and Systems*, 2001, pp. 195–201.
- [2] H. Moon and J. Luntz, "Distributed manipulation of flat objects with two airflow sinks," *IEEE Transactions on robotics*, vol. 22, no. 6, pp. 1189–1201, 2006.
- [3] K. Varsos and J. Luntz, "Superposition methods for distributed manipulation using quadratic potential force fields," *IEEE Transactions on robotics*, vol. 22, no. 6, pp. 1202–1215, 2006.
- [4] K. Varsos, H. Moon, and J. Luntz, "Generation of quadratic potential force fields from flow fields for distributed manipulation," *IEEE Transactions on robotics*, vol. 22, no. 1, pp. 108–118, 2006.
- [5] P.-J. Ku, K. T. Winther, and H. E. Stephanou, "Distributed control system for an active surface device," in *Proc. of the IEEE Int. Conf. on Intelligent Robots and Systems*, 2001, pp. 3417–3422.
- [6] M. Hoetzle, T. Dunifon, and L. Rozevink, "Glass transportation system," U.S. Patent 6,505,483, 2003.
- [7] J. A. Paivanas and J. K. Hanssan, "Wafer air film transportation system," U.S. Patent 4,081,201, 1978.
- [8] J. P. Babinski, B. I. Bertelsen, K. H. Raacke, V. H. Sirgo, and C. J. Townsend, "Transport system for semiconductor wafer multiprocessing station system," U. S. Patent 3,976,330, 1976.
- [9] A. Berlin, D. Biegelsen, P. Cheung, M. Fromherz, D. Goldberg, W. Jackson, B. Preas, J. Reich, and L.-E. Swartz, "Motion control of planar objects using large-area arrays of mems-like distributed manipulators," in *Micromechatronics*, 2000.
- [10] D. K. Biegelsen, A. Berlin, P. Cheung, M. P. Fromherz, D. Goldberg, W. B. Jackson, B. Preas, J. Reich, and L.-E. Swartz, "Air-jet paper mover: An example of meso-scale mems," in *SPIE Int. Symposium on Micromachining and Microfabrication*, 2000.
- [11] J. van Rij, J. Wesselingh, R. A. J. van Ostayen, J. Spronck, R. M. Schmidt, and J. van Eijk, "Planar wafer transport and positioning on an air film using a viscous traction principle," *Tribology International*, vol. 42, pp. 1542–1549, 2009.
- [12] Y. Fukuta, Y.-A. Chapuis, Y. Mita, and H. Fujita, "Design, fabrication and control of mems-based actuator arrays for air-flow distributed micromanipulation," *IEEE/ASME Journal of Microelectromechanical Systems*, vol. 15, no. 4, pp. 912–926, 2006.
- [13] R. Zeggari, R. Yahiaoui, J. Malapert, and J.-F. Manceau, "Design and fabrication of a new two-dimensional pneumatic micro-conveyor," *Sensors & Actuators: A. Physical*, vol. 164, pp. 125–130, 2010.
- [14] A. Delettre, G. J. Laurent, and N. L. Fort-Piat, "A new contactless conveyor system for handling clean and delicate products using induced air flows," in *Proc. of the IEEE Int. Conf. on Intelligent Robots and Systems*, 2010, pp. 2351–2356.
- [15] G. J. Laurent, A. Delettre, and N. L. Fort-Piat, "A new aerodynamic traction principle for handling products on an air cushion," *IEEE Transactions on robotics*, vol. 27, p. 2, 2011.
- [16] G. N. Abramovich, *The theory of turbulent jets*. MIT Press, 1963.
- [17] J. H.-W. Lee and V. Chu, *Turbulent Jets and Plumes: A Lagrangian Approach*. Springer, 2003.
- [18] J. Reed and S. Miles, "High-speed conveyor junction based on an air-jet floatation technique," *Mechatronics*, vol. 14, pp. 685–699, 2004.
- [19] F. M. White, *Fluid Mechanics*. McGraw-Hill Science/Engineering/Math, 2002.